

Finite Volume Simulation of Steady Laminar Natural Convection Heat Transfer Through a Mercury –filled Triangular Enclosure with an Isothermal Cold Side Walls and an Isothermal Hot Bottom Wall.

By :

Dr. Ahmed Kadhim Hussein

Lecturer-College of Engineering-Mechanical Engineering Department
Babylon University- Babylon City – Hilla – Iraq.

Abstract:

Thermal and flow fields due to laminar steady natural convection in a triangular enclosure having thick conducting sidewalls have been investigated numerically. Inclined left and right side walls are maintained at isothermal cold temperatures while the bottom wall is maintained at isothermal hot temperature. Problem has been analyzed and the non-dimensional governing equations are solved using finite volume approach and employing more nodes at the fluid – solid interface. Triangular enclosure is assumed to be filled with mercury as a liquid metal with a Prandtl number of **0.026**. Rayleigh number varies from 10^4 to 10^6 where the flow and thermal fields are computed for various Rayleigh numbers. Consequently, it was observed that the stream function and temperature contours strongly change with high Rayleigh number. The streamline and isotherm plots and the variations of the average Nusselt number at the hot bottom wall and the cold inclined side walls are also presented. The results explained a good agreement with another published results.

الخلاصة:

انسياب الجريان والحرارة نتيجة الحمل الحر الطبقي المستقر خلال دهليز مثلث الشكل بجدران جانبية سميكة وموصلة للحرارة تم تمثيلها عدديا . الجدران المائلان الأيسر و الأيمن يكونان عند درجة حرارة باردة بينما الجدار السفلي يكون عند درجة حرارة ساخنة . المشكلة تم تحليلها والمعادلات اللابعديّة الحاكمة تم حلها باستخدام طريقة الحجم المحددة مع مراعاة استخدام نقاط شبكية مكثفة عند مناطق تماس المائع بالجدار . الدهليز المثلثي مملوء بالزئبق كسائل معدني ويرقم براندل يساوي **0.026**. رقم رايلي يتغير بمدى من 10^4 الى 10^6 حيث مجالات الجريان والحرارة تم حسابها لقيم مختلفة من رقم رايلي. بناء على ذلك لوحظ أن خطوط دالة الجريان والحرارة تتغير بشدة مع قيم رقم رايلي العالية. أشكال خطوط الجريان والحرارة وتغير رقم نسلت المتوسط عند الجدار السفلي الساخن و الجدران الجانبيان المائلان والباردان تم عرضها أيضا . النتائج أوضحت تطابق جيد مع النتائج الأخرى المنشورة.

Keywords: Natural convection, Liquid metal, Laminar Flow, CFD, Steady Flow, Triangular Enclosure.

| Nomenclature | | |
|----------------------|--|-------------|
| Symbol | Description | Unit |
| a_1, a_2 | <i>Transformation coefficients</i> | |
| F | <i>Control function</i> | |
| g | <i>Gravitational acceleration</i> | m/s^2 |
| J | <i>Jacobian of residual equations</i> | |
| H | <i>Height of the triangular enclosure</i> | m |
| Nu_{av} | <i>Average Nusselt number</i> | |
| Nu_x | <i>Local Nusselt number along the side walls</i> | |
| P | <i>Dimensionless pressure</i> | |
| p | <i>Pressure</i> | N/m^2 |
| Pr | <i>Prandtl number</i> | |
| Q | <i>Control function</i> | |
| Ra | <i>Rayleigh number</i> | |
| S_N | <i>Source term due to non orthogonal characteristic of grid system</i> | |
| s_ϕ | <i>Linearized source term for ϕ</i> | |
| T | <i>Temperature</i> | $^\circ C$ |
| T_h | <i>Temperature of the hot surface</i> | $^\circ C$ |
| T_c | <i>Temperature of the cold surface</i> | $^\circ C$ |
| U | <i>Dimensionless velocity component in x-direction</i> | |
| U_{co} | <i>Contravariant velocity component in x-direction</i> | m/s |
| u | <i>Velocity component in x-direction</i> | m/s |
| V | <i>Dimensionless velocity component in y-direction</i> | |
| V_{co} | <i>Contravariant velocity component in y-direction</i> | m/s |
| v | <i>Velocity component in y-direction</i> | m/s |
| X | <i>Dimensionless Coordinate in horizontal direction</i> | |
| x | <i>Cartesian coordinate in horizontal direction</i> | m |
| Y | <i>Dimensionless Coordinate in vertical direction</i> | |
| y | <i>Cartesian coordinate in vertical direction</i> | m |
| W | <i>Width of the triangular enclosure</i> | m |
| Greek Symbols | | |
| α | <i>Thermal diffusivity</i> | m^2/s |
| β | <i>Volumetric coefficient of thermal expansion</i> | K^{-1} |
| θ | <i>Dimensionless temperature</i> | |
| ϕ | <i>Variable vector</i> | |
| Γ_ϕ | <i>Diffusion coefficient</i> | |
| ν | <i>Kinematic viscosity of the fluid</i> | m^2/s |
| ρ | <i>Density of the fluid</i> | kg/m^3 |
| ζ, η | <i>Dimensionless body-fitted coordinates</i> | |

1. Introduction.

The phenomenon of natural convection heat transfer and fluid flow or some times called buoyancy-driven flow in enclosures has been studied extensively in recent years in response to energy-related applications, such as thermal insulation of buildings using air gaps, solar energy collectors, furnaces and fire control in buildings. Most of the geometrical configurations of enclosures in the previous studies are focused on rectangular or square enclosure. However, the shape of enclosure can be in different configurations such as, in most of the related engineering situations which include triangle, parallelogram or trapezoidal. Modeling natural convection inside a triangular enclosure, previously reported in the literature employed a symmetry condition at the midplane and performed the simulations using only one half of the physical domain **Tamanna et al. , 2008**. **Akinsete and Coleman, 1982**, used a finite difference representation of the steady-state stream function, vorticity and energy equations with an adiabatic boundary condition for the vertical wall in a right triangular enclosure. They recognized the existence of unbounded heat transfer at the corner of the enclosure where a temperature discontinuity exists and calculated the limiting value of Nusselt number. **Del Campo et al. , 1988**, modeled natural convection in triangular enclosures using Galerkin finite element method with a stream function – vorticity formulation of steady state equations of motion. Their investigation was based on a symmetric boundary condition for a system with heating from below. **Jyotsna and Vanka , 1995**, investigated the steady viscous flow in a triangular cavity by using multigrid calculation. They found that the bi-quadratic elements with lesser number of nodes smoothly capture the non-linear variations of the field variables which were in contrast with finite difference / finite volume solutions available. **Asan and Namli , 2000**, carried out a numerical study for the two- dimensional laminar natural convection in a pitch roof of triangular cross-section under summer day boundary condition. They investigated the effects of height-base ratio and Rayleigh number on the flow structure and heat transfer. They found that a considerable proportion of the heat transfer across the base wall of the region takes place near the intersection of the cold horizontal wall and hot inclined wall.

Chengwang and **Patterson** , **2002**, carried out both analytically and numerically the unsteady natural convection in a triangular domain induced by the absorption of solar radiation. Their work consisted of two parts: a scaling analysis and a numerical simulation. The scaling analysis for small bottom slopes revealed that a number of flow regimes were possible depending on the Rayleigh number and the relative value of certain non-dimensional parameters describing the flow. They classified the flow into a conductive, a transitional or a convective regime determined merely by the Rayleigh number. Proper scales have been established to quantify the flow properties in each of these flow regimes. Their numerical simulation verified the scaling results. **El Hassan et al.** , **2005** , performed a numerical computation of laminar natural convection in a gamma of right-angled triangular cavities filled with air. The vertical walls were heated and the inclined walls were cooled while the upper connecting walls were insulated from the ambient air. The defining apex angle was located at the lower vertex formed between the vertical and inclined walls.

The finite volume method was used to perform the computational analysis encompassing a collection of apex angles compressed in the interval that extends from 5° to 63° . The height-based Rayleigh number, being unaffected by the apex angle ranges from a low 10^3 to a high 10^6 . Numerical results were reported for the velocity field , the temperature field and the mean convective coefficient along the heated vertical wall. A correlation equation was constructed and also a figure of merit ratio between the average Nusselt number and the cross sectional area of the cavity was proposed.

Roy et al.¹, **2008**, used a penalty finite element analysis with bi-quadratic elements to investigate natural convection flows within an isosceles triangular enclosure with an aspect ratio of **0.5**. Two cases of thermal boundary conditions were considered with uniform and non-uniform heating of bottom wall. The numerical solution of the problem was illustrated for Rayleigh numbers (**Ra**), $10^3 \leq \mathbf{Ra} \leq 10^5$ and Prandtl numbers (**Pr**), $0.026 \leq \mathbf{Pr} \leq 1000$. They found that the intensity of circulation was to be larger for non-uniform heating at a specific **Pr** and **Ra**. Multiple circulation cells were found to occur at the central and corner regimes of the bottom wall for a small Prandtl number regime (**Pr =0.026-0.07**) also they observed the oscillatory distribution of the local Nusselt number. In

contrast, the intensity of primary circulation was found to be stronger, and secondary circulation was completely absent for a high Prandtl number regime ($\text{Pr} = 0.7-1000$). Some correlations were proposed for the average Nusselt number in terms of the Rayleigh number for a convection dominant region with higher Prandtl numbers. **Roy et al.², 2008**, studied numerically the natural convection in a right-angle triangular enclosure filled with a porous matrix. A penalty finite element analysis with bi-quadratic trapezoidal elements was used for solving the Navier-Stokes and energy balance equations. Their study was carried out in two cases, depending on various thermal boundary conditions. The first when the vertical wall was uniformly or linearly heated, while the inclined wall was cold isothermal and the second when the inclined wall was uniformly or linearly heated, while the vertical wall was cold isothermal. In all cases, the horizontal bottom wall was considered adiabatic, and the geometric aspect ratio was considered to be **1.0**. It has been found that at low Darcy numbers ($\text{Da} \leq 10^{-5}$), the heat transfer was primarily due to conduction, irrespective of the **Ra** and **Pr**. As Rayleigh number increases, there was a change from a conduction-dominant region to a convection-dominant region for $\text{Da} = 10^{-3}$. The results were presented in the form of the stream function and isotherm contours. It was observed that the average Nusselt number for the vertical wall was $\sqrt{2}$ times that of the inclined wall for all studied cases. **Basak et al., 2008**, used a penalty finite element analysis with bi-quadratic elements to investigate the effects of uniform and non-uniform heating of inclined walls on natural convection flows within a isosceles triangular enclosure. Two cases of thermal boundary conditions were considered. The first case when two inclined walls were uniformly heated while the bottom wall was cold isothermal and the second when the two inclined walls were non-uniformly heated while the bottom wall was cold isothermal. The numerical solution of the problem was presented for the range Rayleigh numbers (**Ra**), $10^3 \leq \text{Ra} \leq 10^6$ and the Prandtl numbers (**Pr**), ($0.026 \leq \text{Pr} \leq 1000$). It has been found that at small Prandtl numbers, geometry does not have much influence on flow structure while at $\text{Pr} = 1000$, the stream function contours were nearly triangular showing that geometry has considerable effect on the flow pattern. They noticed that the non-uniform heating produced greater heat transfer rates at the center of the walls than the uniform heating.

The major purpose of the current work is to compute the thermal and flow fields due to laminar steady natural convection in a mercury-filled triangular enclosure where their inclined left and right side walls are maintained at isothermal cold temperatures while the bottom wall is maintained at isothermal hot temperature. The computations are carried out for different Rayleigh number ranging from 10^4 to 10^6 . The current study is based on the configuration of **Basak et al. , 2008**. The major difference between **Basak et al. , 2008** and the present work is that the present work deals with the inclined isothermal cold temperatures side walls while the bottom wall is maintained at isothermal hot temperature using finite volume method rather than the uniform and non-uniform heating of inclined walls while the bottom wall is cold isothermal using finite element method as in **Basak et al. ,2008** work.

2. Geometry Description, Mathematical Modeling and Assumptions.

The geometry under investigation is a triangular enclosure filled with mercury which its bottom is maintained at a uniform hot temperature (T_h). The right and left side walls of the enclosure are maintained at a uniform cold temperature (T_c). The geometry under consideration is shown schematically in **Fig.1**. The triangular enclosure has a height (H) and a base (W) and the mercury is chosen as a working fluid with Prandtl number $P_r = 0.026$. The flow and thermal fields are described by continuity, momentum and energy equations. These equations are written in a dimensionless form by dividing all dependent and independent variables by suitable constant terms. The solution is obtained using a finite volume scheme and the following assumptions are considered :-

- a. The flow is considered steady , laminar and two-dimensional.
- b. The fluid properties are assumed constant except for the density variation which is treated according to Boussinesq approximation.
- c. The fluid inside the triangular enclosure is assumed Newtonian while viscous dissipation effects are considered negligible.

The viscous incompressible flow and the temperature distribution inside the enclosure are described

by the Navier–Stokes and the energy equations, respectively. The governing equations are transformed into a dimensionless forms under the following non-dimensional variables **Basak et al. , 2008**

$$\theta = \frac{T - T_c}{T_h - T_c}, \quad X = \frac{x}{W} \quad \text{and} \quad Y = \frac{y}{H} \quad (1)$$

$$P = \frac{\rho H^2}{\rho \alpha^2}, \quad U = \frac{uW}{\alpha} \quad \text{and} \quad V = \frac{vH}{\alpha} \quad (2)$$

where **X** and **Y** are the dimensionless coordinates measured along the horizontal and vertical axes, respectively, **u** and **v** being the dimensional velocity components along **x** and **y** axes, and **θ** is the dimensionless temperature. The dimensionless forms of the governing equations under steady

state condition are expressed in the following forms **Basak et al. , 2008** :

$$\frac{\partial U}{\partial X} + \frac{\partial V}{\partial Y} = 0 \quad (3)$$

$$U \frac{\partial U}{\partial X} + V \frac{\partial U}{\partial Y} = -\frac{\partial P}{\partial X} + \text{Pr} \left(\frac{\partial^2 U}{\partial X^2} + \frac{\partial^2 U}{\partial Y^2} \right) \quad (4)$$

$$U \frac{\partial V}{\partial X} + V \frac{\partial V}{\partial Y} = -\frac{\partial P}{\partial Y} + \text{Pr} \left(\frac{\partial^2 V}{\partial X^2} + \frac{\partial^2 V}{\partial Y^2} \right) + \text{RaPr} \theta \quad (5)$$

$$U \frac{\partial \theta}{\partial X} + V \frac{\partial \theta}{\partial Y} = \left(\frac{\partial^2 \theta}{\partial X^2} + \frac{\partial^2 \theta}{\partial Y^2} \right) \quad (6)$$

where **U** and **V** being the non-dimensional velocity components along **X** and **Y** axes respectively, **P** is the dimensionless pressure, **Pr** is the Prandtl number and **Ra** is the Rayleigh number. The previous dimensionless numbers are defined by **Arpaci and Larsen ,1984** :-

$$\text{Pr} = \frac{\nu}{\alpha} \quad \text{and} \quad \text{Ra} = \frac{g\beta(T_h - T_c)H^3}{\nu^2} \text{Pr} \quad (7)$$

Where , **β** is the volumetric coefficient of thermal expansion and **g** is the gravitational acceleration. The average Nusselt number at the cold right and left side walls and the hot bottom wall are given by **Basak et al. , 2008**:-

$$Nu_{av})_{sidewalls} = \frac{1}{\sqrt{2}} \int_0^{\sqrt{2}} Nu_x]_{Side} dH \quad (8-a)$$

$$Nu_{av})_{bottomwall} = \frac{1}{2} \int_0^2 Nu_x]_{Bottom} dX \quad (8-b)$$

Where, dH represents the elemental height along the left and right side walls and Nu_x is the local Nusselt number along the side walls and bottom wall respectively.

3. Boundary conditions.

The boundary conditions which are used in the present work can be summarized as follows:-

1. The bottom wall is maintained at a uniform hot temperature, so:

$$Y = 0.0 \quad \theta = 1.0 \quad \text{and} \quad U = V = 0.0 \quad (9)$$

2. The left side wall is maintained at a uniform cold temperature, so:

$$\text{at} \quad X = 0.0 \quad \theta = 0.0 \quad \text{and} \quad U = V = 0.0 \quad (10)$$

3. The right side wall is maintained at a uniform cold temperature, so:

$$\text{at} \quad X = 1 \quad \theta = 0.0 \quad \text{and} \quad U = V = 0.0 \quad (11)$$

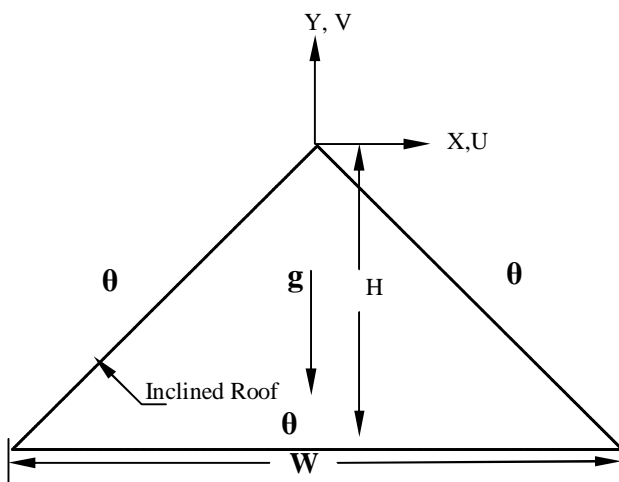


Fig. 1: Physical configuration and boundary conditions of the triangular enclosure.

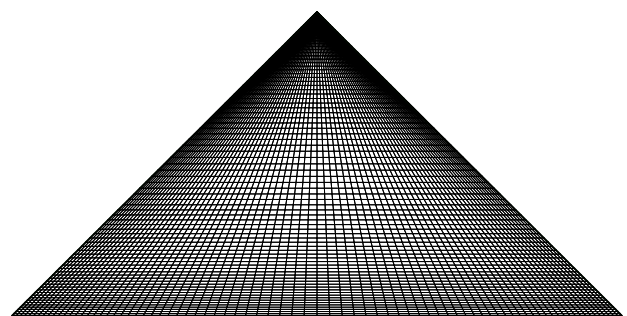


Fig. 2 A 2D - grid distribution (90x90) with non-uniform and non-orthogonaldistributions for the triangular enclosure.

4. Numerical Scheme.

The grid generation calculation is based on the curvilinear coordinate system applied to fluid flow as described by **Thompson et al.,1974**. **Fig.2** shows the schematic of two dimensions body fitting grid used for the present computation. This grid is obtained by solving non-homogeneous **2-D** Poisson equations:-

$$\xi_{xx} + \xi_{yy} = F(\xi, \eta) \quad (12)$$

$$\eta_{xx} + \eta_{yy} = Q(\xi, \eta) \quad (13)$$

where **F** and **Q** are control functions used to cluster the grid near the walls. The reason is to predict the velocity gradient because there is a friction between the wall and the fluid. The equations are transformed to (ξ, η) coordinates by interchanging the roles of dependent variables. This yield the following system equations:-

$$g_{11}x_{\xi\xi} - g_{21}x_{\xi\eta} + g_{22}x_{\eta\eta} = -J^2(F_{x\xi} + Q_{x\eta}) \quad (14)$$

$$g_{11}y_{\xi\xi} - g_{21}y_{\xi\eta} + g_{22}y_{\eta\eta} = -J^2(F_{y\xi} + Q_{y\eta}) \quad (15)$$

Where:

$$g_{11} = x_{\eta}^2 + y_{\eta}^2$$

$$g_{21} = 2(x_{\xi}x_{\eta} + y_{\xi}y_{\eta})$$

$$g_{22} = x_{\xi}^2 + y_{\xi}^2$$

$$J = x_{\xi}y_{\eta} - x_{\eta}y_{\xi}$$

The steady-state governing equations (3 to 6) are solved by using the finite-volume method using Patankar's algorithm **Patankar,1980**. A two-dimensional non-uniformly collocated grid system is used. These equations can be written in a general transport equation as follows **Patankar,1980**: -

$$\frac{\partial(\rho u \phi)}{\partial x} + \frac{\partial(\rho v \phi)}{\partial y} = \frac{\partial}{\partial x} \left[\Gamma_{\phi} \left(\frac{\partial \phi}{\partial x} \right) \right] + \frac{\partial}{\partial y} \left[\Gamma_{\phi} \left(\frac{\partial \phi}{\partial y} \right) \right] + S_{\phi} \quad (16)$$

This equation represents a starting point for computational procedure in (FVM) (**Ferziger** and **Peric, 1999**).The flow domain is subdivided into a number of control volumes with a nodal point at the center of each control volume and the set of governing equations are integrated over the control volumes, which produces a set of algebraic equations. The simple algorithm is used to solve the coupled system of governing equations and the set of algebraic equations are solved sequentially. A second-order upwind differencing scheme is used for the formulation of the convection contribution to the coefficients in the finite-volume equations. Central

differencing is used to discretize the diffusion terms, while a blending of up-wind and central differencing is used for the convection terms. The computation is terminated when the residuals for the continuity and momentum equations get below 10^{-5} and the residual for the energy equation gets below 10^{-8} . For the general curvilinear coordinates system (ξ, η) , the general transport equation (eqs.(12) and (13)) can be transformed to the following form:-

$$\frac{\partial}{\partial \xi} (\rho U_{co} \phi - \frac{a_1 \Gamma \phi}{J} \frac{\partial \phi}{\partial \xi}) + \frac{\partial}{\partial \eta} (\rho V_{co} \phi - \frac{a_2 \Gamma \phi}{J} \frac{\partial \phi}{\partial \eta}) = S_{new} \quad (17)$$

where (U_{co}, V_{co}) are the contravariant velocity components and $S_{NEW} = J S_{\phi} + S_N$ where S_N is the source term due to non-orthogonal characteristic of grid system. Also, the transformation coefficients (a_1, a_2) are defined as **Hoffmann, 1989**:-

$$\begin{aligned} a_1 &= \xi_x^2 + \xi_y^2 \\ a_2 &= \eta_x^2 + \eta_y^2 \end{aligned} \quad (18)$$

While the transformation metrics are computed as follows **Hoffmann, 1989**:-

$$\eta_y = -\frac{x_{\xi}}{J} \text{ and } \eta_x = -\frac{y_{\xi}}{J}, \quad \xi_x = \frac{y_{\eta}}{J}, \quad \xi_y = -\frac{x_{\eta}}{J} \quad (19)$$

5. Grid Sensitivity Test.

The numerical scheme used to solve the governing equations for the current work is a finite volume approach. It provides smooth solutions at the interior domain including the corners. The enclosure is meshed with a non-uniform grid with a very fine spacing near the corners. As shown in **Fig.2**, the **2-D** computational grids are clustered towards the corners. The location of the nodes is calculated using a stretching function so that the node density is higher near the walls of the enclosure. Solutions are assumed to converge when the following convergence criteria is satisfied at every point in the solution domain :-

$$\left| \frac{\phi_{new} - \phi_{old}}{\phi_{old}} \right| \leq 10^{-5} \quad (20)$$

Where represents a dependent variable U , V , P and θ . In order to obtain grid independent solution, a grid refinement study is performed for uniformly heated bottom wall, $\theta(X,0) = 1$, and cold inclined side walls, $\theta(X,Y) = 0$, inside the triangular enclosure with $Ra = 10^5$ and $Pr = 0.026$. In the current work, eight combinations (40x40, 50x50, 60x60, 70x70, 80x80, 90x90, 100x100 and 120x120) of control volumes are used to test the effect of grid size on the accuracy of the predicted results. Fig. 3 shows the convergence of the average Nusselt number Nu_{av} at the heated surface of bottom wall with grid refinement. It is observed that grid independence is achieved with a combination of 90 x 90 control volumes where there is insignificant change in the average Nusselt number Nu_{av} . Therefore, it is shown that the high mesh refinement provides a good result in the present work.

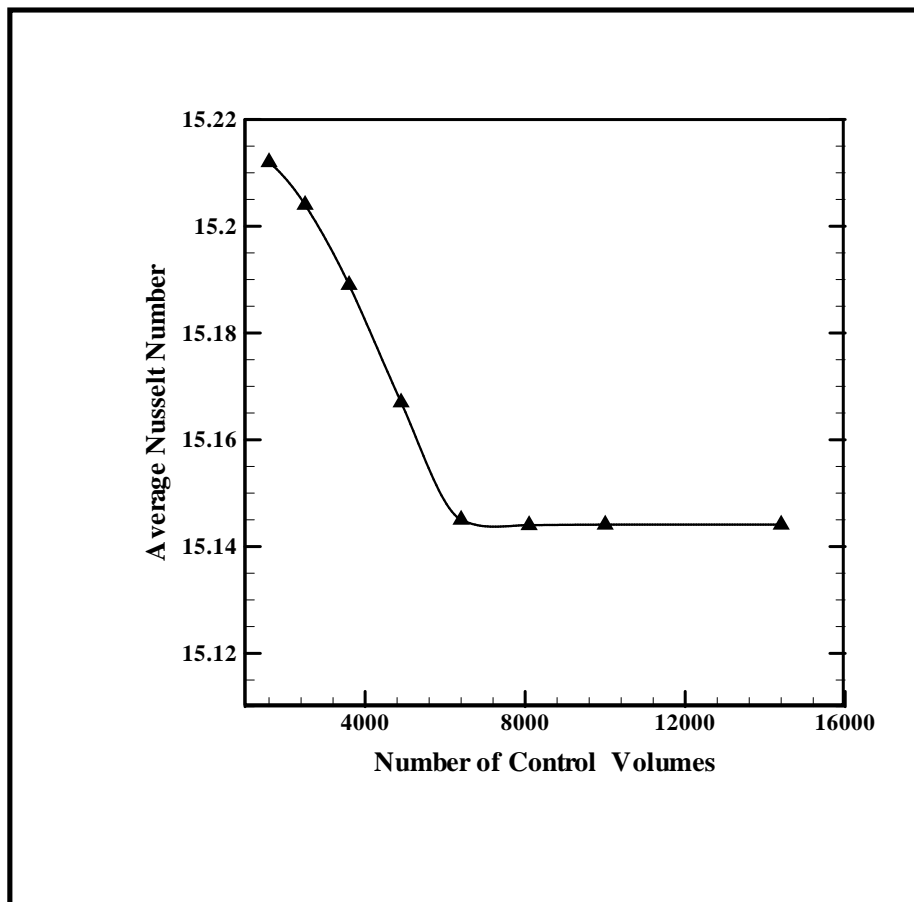


Fig. 3. Variation of average Nusselt number along a heated bottom wall as a function of control volume for a triangular enclosure with uniformly heated bottom wall and cold inclined side walls at $Ra = 10^5$ and $Pr = 0.026$.

6. Numerical Results Validation.

For the purpose of the present numerical algorithm validation, a laminar natural convection problem inside the same tested model as obtained by **Basak et al., 2008**, where the effects of uniform heating of inclined walls while the bottom wall is cold isothermal in a triangular enclosure is tested. The comparison is made for various Rayleigh number (**Ra**), ($10^4 \leq \mathbf{Ra} \leq 10^6$) and Prandtl number (**Pr = 0.026**). The program solution algorithm has been validated by performing calculations for the average Nusselt numbers along the uniformly heated inclined walls and cold bottom wall and the results are shown in **Table 1**. A good agreement is seen between the present computation and the previous values by **Basak et al., 2008**, with a maximum deviation less than 1%. Additional validation is performed by using the present numerical algorithm to investigate the same problem considered by **Basak et al., 2008**, using the same flow conditions, geometry, and the boundary conditions but the numerical scheme is different. Again good agreement is achieved between **Basak et al., 2008**, and the present numerical scheme for both the streamlines and temperature contours as shown in **Fig.4**. These validations make a good confidence in the present numerical model to deal with the same triangular enclosure configuration problem for calculating the flow and thermal fields for the present geometry and boundary conditions.

Table 1

Comparison of the present average Nusselt number along the uniformly heated inclined walls and cold bottom wall for triangular enclosure filled with mercury ($Pr = 0.026$) with those of previous studies.

| <i>Ra</i> | Inclined Walls | | | Bottom Wall | | |
|-----------|--------------------|--------------|---------|---------------------|--------------|---------|
| | Basak et al., 2008 | Present work | Error % | Basak et al., 2008, | Present work | Error % |
| 1000 | 5.541062 | 5.554477 | 0.242 | 3.7434 | 3.7734 | 0.801 |
| 20000 | 5.576833 | 5.582317 | 0.010 | 3.7912 | 3.8071 | 0.419 |
| 100000 | 5.668227 | 5.698325 | 0.530 | 3.8757 | 3.8805 | 0.123 |
| 700000 | 5.780730 | 5.795118 | 0.249 | 3.8841 | 3.9037 | 0.504 |
| 1000000 | 5.801592 | 5.823398 | 0.375 | 3.8972 | 3.9087 | 0.295 |

7. Results and Discussion.

The properties of the laminar flow and thermal fields under steady state conditions in a triangular enclosure which is heated from bottom wall while the right and left side walls of the enclosure is maintained at a uniform cold temperatures are examined by investigating the effects of the Rayleigh number (**Ra**). In the current numerical investigation, the following domains of the dimensionless groups are considered: Rayleigh number (**Ra**), 2×10^4 , 10^5 , 7×10^5 and 10^6 while Prandtl number (**Pr** = **0.026**).

7.1 Effect of Rayleigh number.

The stream lines and isotherms at different Rayleigh number ranging from 10^4 to 10^6 are shown in **Figures (5 and 6)** when the left and right side walls are maintained at cold temperatures respectively while the bottom wall is maintained at hot temperature. The temperature of the fluid near the bottom wall of the enclosure is higher than the temperature of the fluid near the cold right and left side walls, so the fluid near the bottom wall have lower density than those near the cold right and left side walls. For this reason, the fluid near the hot bottom wall move upward and is fallen downward near the cold right and left side walls resulting a rotating circulations in the enclosure where the center of vortices located at the half of the enclosure. When the values of Rayleigh number are low (i.e,when **Ra** = 2×10^4 and 10^5) as shown in **Fig.5**.The isotherms are smooth and approximately parallel which covering all the size of the enclosure indicating that the heat transfer mechanism is due to conduction heat transfer and the temperature distribution is similar to that with stationary fluid .Also, it can be observed that the values of the temperature contours are increased from the low values at cold right and left side walls to high values at bottom wall which satisfying the problem boundary conditions. When the values of the Rayleigh number increases (i.e,when **Ra** = 7×10^5 and 10^6) as shown in **Fig.6**.The fluid circulation inside the enclosure is strongly dependent on Rayleigh number where a circulation flow region of high intensity can be observed close to the bottom wall and push the fluid towards the center of the enclosure.Also, a clear deformation in stream lines can be detected as shown in **Fig.6**.From the other hand, The effect of significant natural convection is also exhibited in the temperature contours which begin to deform and move towards the central part of the bottom wall.

Also, a secondary circulations can be noticed at the upper and lower regions of the enclosure due to enhanced convection from the bottom wall of the enclosure. Also, it can be observed that the size of the primary vortex decreases with the increase of Rayleigh number, while the secondary vortices size increase with the increase of Rayleigh number. Finally, multiple circulation vortices are found to occur at the central and corner regions of the bottom wall for a small Prandtl number fluid, and in general the circulation does not have the triangular shape so it has been found that at small Prandtl number fluid, the geometry of the enclosure does not have much effect on flow structure.

7.2 The Variation of the Average Nusselt number.

Figures (7 and 8) explain the average Nusselt number variations along the hot bottom wall and the cold right and left inclined side walls respectively for various Rayleigh number. From these figures, it is seen that the average Nusselt number increases significantly with Rayleigh number. It may be noticed also that the overall heat transfer rate (average Nusselt number) is less for the cold right and left inclined side walls as compared to the bottom wall. The reason of this behaviour is due to high heat input for the hot bottom wall. Also, it has been observed that as Rayleigh number increases, the values of average Nusselt number increases also which indicate that there is a clear change from a conduction-dominant region to a convection-dominant region

8. Conclusions.

The following conclusions may be drawn from the results of the present work:

1- When the values of Rayleigh number are low (i.e, $\mathbf{Ra} = 2 \times 10^4$ and 10^5).The isotherms are smooth and approximately parallel which covering all the size of the enclosure indicating that the heat transfer mechanism is due to conduction. Also, a rotating circulations with small magnitudes of the stream function are observed in the enclosure where the center of vortices located at the half of the enclosure.

2-When the values of the Rayleigh number increases (i.e,when $\mathbf{Ra} = 7 \times 10^5$ and 10^6).The fluid circulation inside the enclosure is strongly dependent on Rayleigh number where a circulation flow region of high intensity can be observed close to the bottom wall and push the fluid towards the center of the enclosure. From the other

hand, The effect of significant natural convection is also exhibited in the temperature contours which begin to deform and move towards the central part of the bottom wall.

3- A secondary circulations can be noticed at the upper and lower regions of the enclosure due to enhanced convection from the bottom wall of the enclosure. Also, it can be observed that the size of the primary vortex decreases with the increase of Rayleigh number, while the secondary vortices size increase with the increase of Rayleigh number.

4- Multiple circulation vortices are found to occur at the central and corner regions of the bottom wall for a small Prandtl number fluid and in general the circulation does not have the triangular shape so it has been found that at small Prandtl number fluid, the geometry of the enclosure does not have much effect on flow structure.

5- The average Nusselt number increases significantly with Rayleigh number. It may be noticed also that the overall heat transfer rate (average Nusselt number) is less for the cold right and left inclined side walls as compared to the hot bottom wall. The reason of this behaviour is due to high heat input for the hot bottom wall. Also, it has been noticed that as Rayleigh number increases, the values of average Nusselt number increases also which indicate that there is a clear change from a conduction-dominant region to a convection-dominant region.

Referencers.

Akinsete, V. and Coleman, T. "Heat Transfer by Steady Laminar Free Convection in Triangular Enclosures", *International Journal of Thermal Sciences*, Vol.25, 1982, pp: 991-998.

Arpaci, P. and Larsen, P. "Convection Heat Transfer", Prentice-Hall, 1984.

Asan, H. and Namli, L. "Laminar Natural Convection in a Pitched Roof Triangular Cross-Section", *Energy Building*, Vol.33, 2000, pp: 69-73.

Basak, T., Roy, S., Babu, K. and Balakrishnan, A. "Finite Element Analysis of Natural Convection Flow in Isosceles Triangular Enclosure Due to Uniform and Non-Uniform Heating at the Side Walls", *International Journal of Heat and Mass Transfer*, Vol.51, 2008, pp: 4496-4505.

Chengwang, L. and Patterson, J. "Unsteady Natural Convection in a Triangular Enclosure Induced by Absorption of Radiation" *Journal of Fluid Mechanics*, Vol.460, No.1, 2002, pp: 181-209.

- Del Campo,E., Sen,E. and Ramos,E.” Analysis of Laminar Natural Convection in a Triangular Enclosure” Numerical Heat Transfer, Vol.13, 1988, pp: 353–372.
- El Hassan,R.,Campo,A. and Chang,J. ” Natural Convection Patterns in Right-Angled Triangular Cavities With Heated Vertical Sides and Cooled Hypotenuses”, Journal of Heat Transfer, Vol. 127,No.10,2005, pp:1181-1186.
- Ferziger, J. and Peric, M., “Computational Methods for Fluid Dynamics”, 2nd Edition Springer Verlag, Berlin Hedelberg, 1999.
- Hoffmann, K.,“Computational Fluid Dynamics for Engineers”, Engineering Education System Publication, U.S.A, 1989.
- Jyotsna,R.and Vanka, S. ”Multigrid Calculation of Steady Viscous Flow in a Triangular Cavity Journal of Computer Physics , Vol.122,1995,pp:107–117.
- Patankar, S.V., “Numerical Heat Transfer and Fluid Flow” , Hemisphere Publishing Corporation, New York, 1980.
- Roy1, S., Tanmay,B.,Thirumalesha,C. and Murali Krishna,C. “Finite Element Simulation on Natural Convection Flow in a Triangular Enclosure Due to Uniform and Non-uniform Bottom Heating”, Journal of Heat Transfer, Vol. 130,No.3,2008, pp:1761-1769.
- Roy2, S., Tanmay,B.,Thirumalesha,C. and Murali Krishna,C. “Finite Element Simulations of Natural Convection in a Right-Angle Triangular Enclosure Filled with a Porous Medium Effects of Various Thermal Boundary Conditions Heating”, Journal of Porous Media, Vol.11,No.2,2008, pp:159-178.
- Tamanna , S. ,Saha, S. , Saha, G.and Quamrul Islam , M. “Natural Convection in Tilted Square Cavities with Triangular Shaped Top Cold Wall “ , Journal of Mechanical Engineering , Vol.ME 39, No.1, 2008, pp:33-42.
- Thompson, P., Thamas, F. and Mastin, F., “Automatic Numerical Generation of Body- Fitted Curvilinear Coordinate System” Journal of computational physics, Vol. 15, 1974, pp: 299-319.

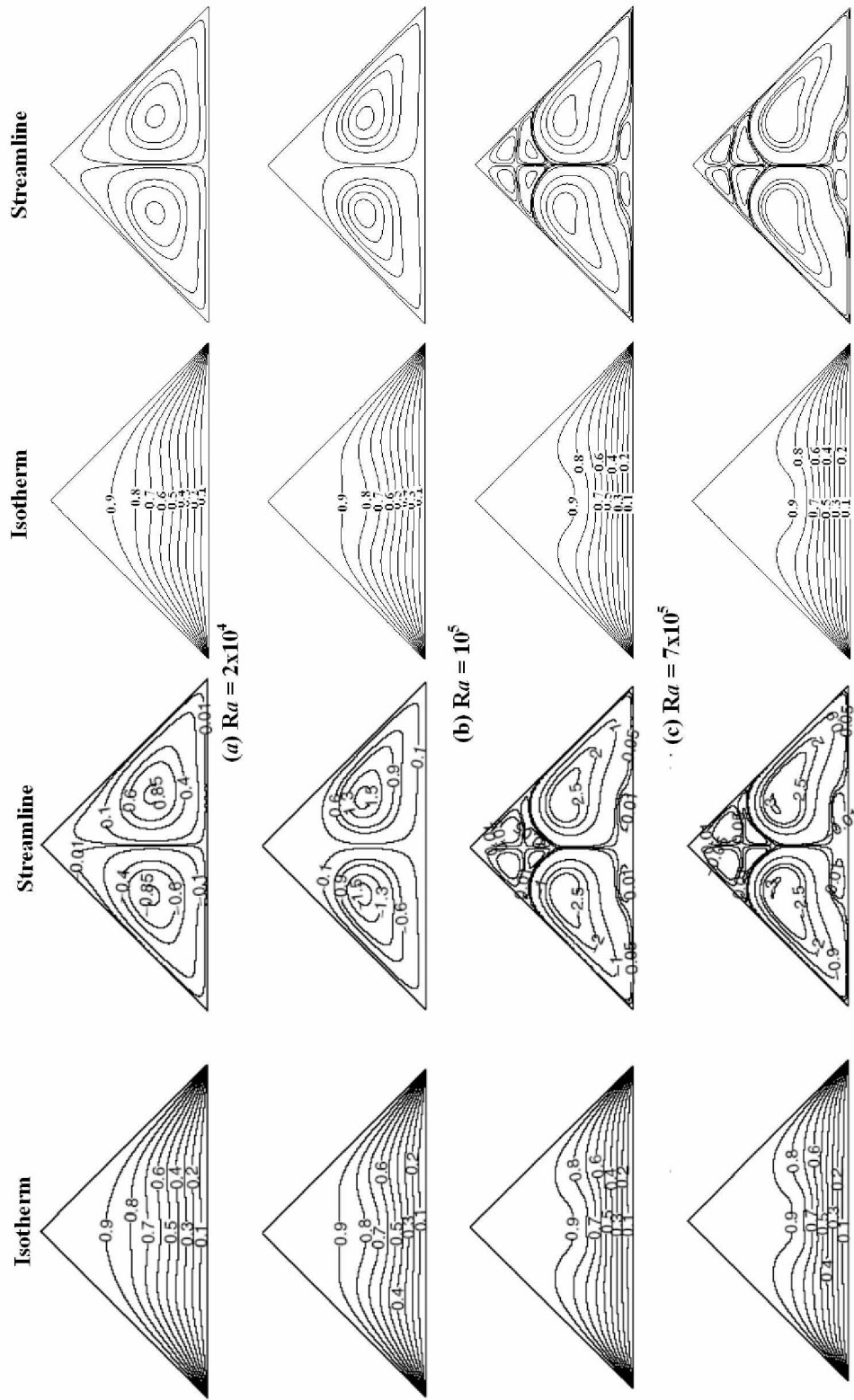


Fig. 4. Comparison of the isotherms and streamlines between the present work (right) and that of **Basak et al.,2008**, (left) for cold bottom wall and the heated inclined walls for a triangular enclosure filled with mercury ($Pr = 0.026$)

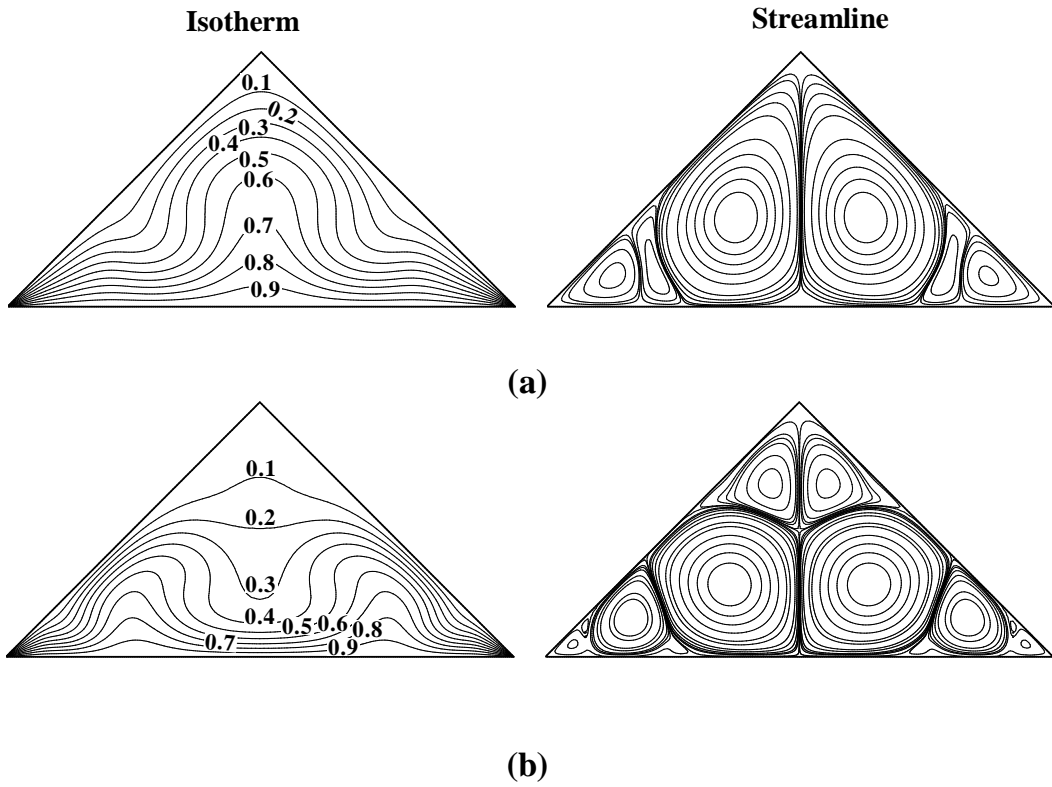


Fig. 5. Temperature and stream function contours for a heated bottom wall and cold inclined side walls for a triangular enclosure with (a) $Ra=2 \times 10^4$ (b) $Ra=10^5$ and $Pr = 0.026$.

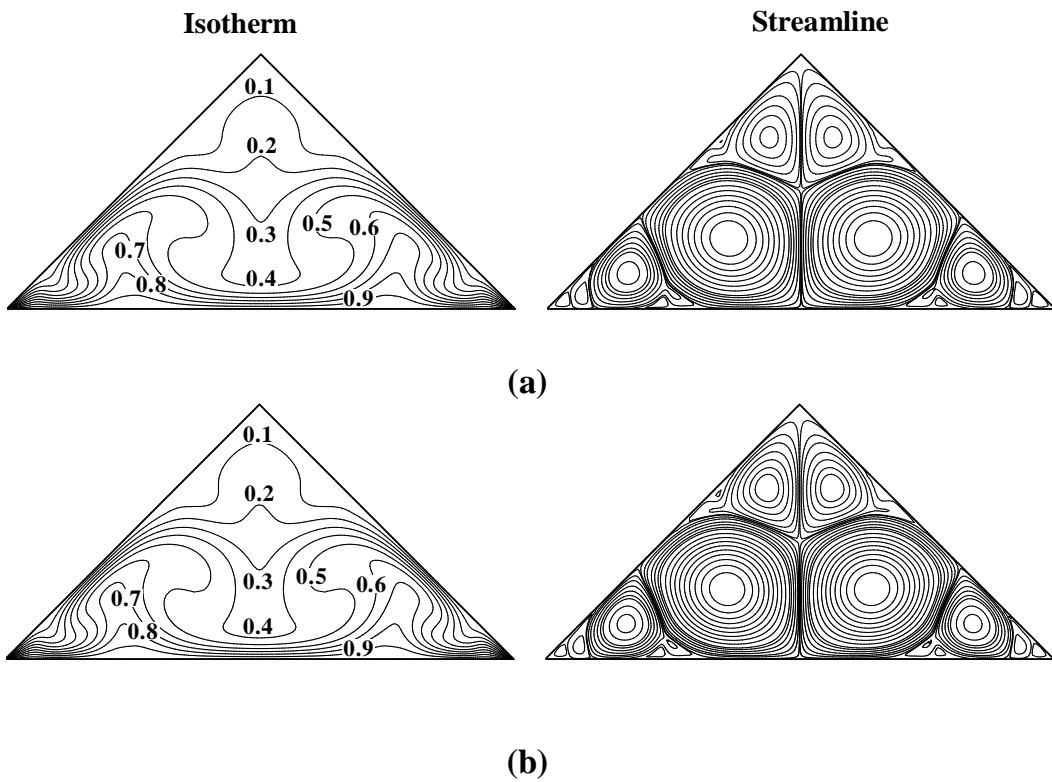


Fig. 6. Temperature and stream function contours for a heated bottom wall and cold inclined side walls for a triangular enclosure with (a) $Ra=7 \times 10^5$ (b) $Ra=10^6$ and $Pr = 0.026$.

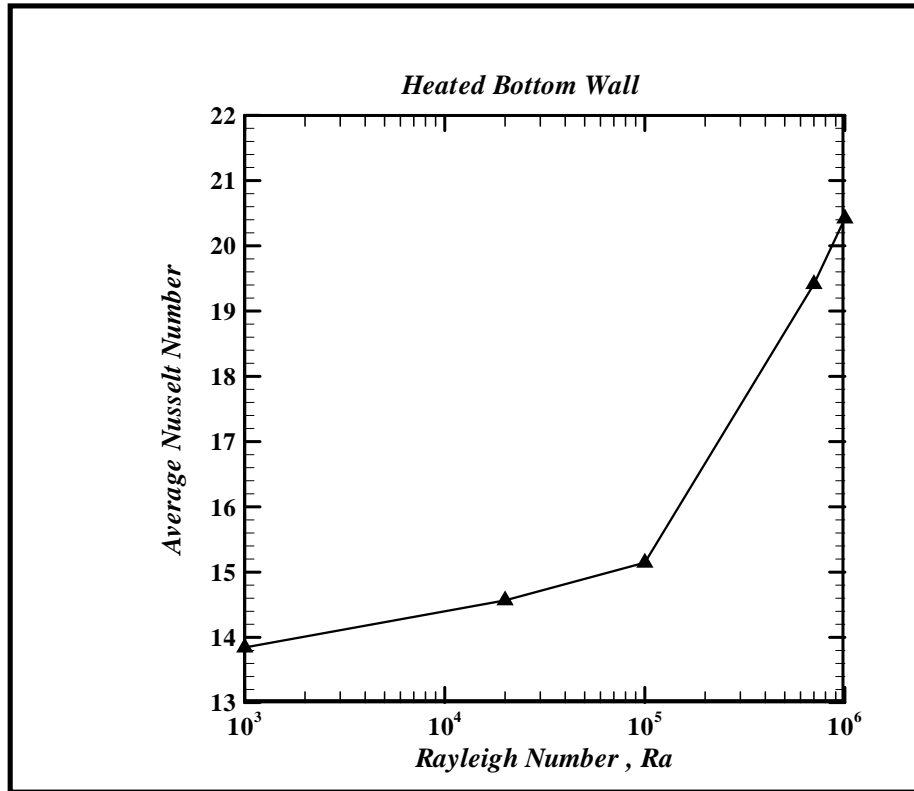


Fig. 7. Variation of average Nusselt number along a heated bottom wall with Rayleigh number for a triangular enclosure with a heated bottom wall and cold inclined side walls at $Pr = 0.026$.

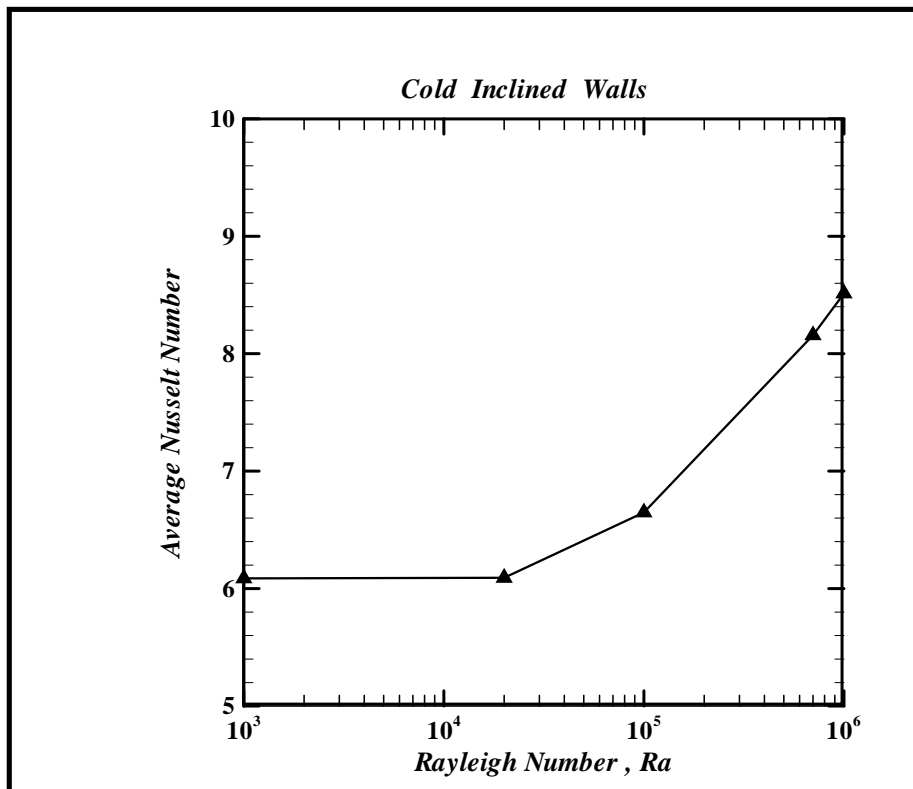


Fig. 8. Variation of average Nusselt number along a cold isothermal inclined walls with Rayleigh number for a triangular enclosure with a heated bottom wall and cold inclined side walls at $Pr = 0.026$.